Ab initio calculations and synthesis of the off-stoichiometric half-Heusler phase $Ni_{1-x}Mn_{1+x}Sb$

Marcus Ekholm, Petter Larsson, Björn Alling, Ulf Helmersson and Igor Abrikosov

Original Publication:

Marcus Ekholm, Petter Larsson, Björn Alling, Ulf Helmersson and Igor Abrikosov, Ab initio calculations and synthesis of the off-stoichiometric half-Heusler phase Ni1-xMn1+xSb, 2010, JOURNAL OF APPLIED PHYSICS, (108), 9, 093712.
http://dx.doi.org/10.1063/1.3476282

Ab initio calculations and synthesis of the off-stoichiometric half-Heusler phase $Ni_{1-x}Mn_{1+x}Sb$

M. Ekholm,[a] P. Larsson, B. Alling, U. Helmersson, and I. A. Abrikosov
Department of Physics, Chemistry and Biology (IFM), Linköping University, SE-58183 Linköping, Sweden

(Received 14 June 2010; accepted 14 July 2010; published online 11 November 2010)

We perform a combined theoretical and experimental study of the phase stability and magnetism of the off-stoichiometric $Ni_{1-x}Mn_{1+x}Sb$ in the half-Heusler crystal phase. Our work is motivated by the need for strategies to engineer the magnetism of potentially half-metallic materials, such as NiMnSb, for improved performance at elevated temperatures. By means of *ab initio* calculations we investigate $Ni_{1-x}Mn_{1+x}Sb$ over the whole composition range $0 \leq x \leq 1$ of Ni replacing Mn and show that at relevant temperatures, the half-Heusler phase should be thermodynamically stable up to at least $x=0.20$ with respect to the competing C38 structure of Mn_2Sb. Furthermore we find that half-Heusler $Ni_{1-x}Mn_{1+x}Sb$ retains half-metallic band structure over the whole concentration range and that the magnetic moments of substitutional Mn_{Ni} atoms display magnetic exchange interactions an order of magnitude larger than the Ni–Mn interaction in NiMnSb. We also demonstrate experimentally that the alloys indeed can be created by synthesizing off-stoichiometric $Ni_{1-x}Mn_{1+x}Sb$ films on MgO substrates by means of magnetron sputtering. © *2010 American Institute of Physics*. [doi:10.1063/1.3476282]

I. INTRODUCTION

NiMnSb has been suggested as a strong candidate material for spintronics applications due to its predicted half-metallic band structure[1] and high Curie temperature (728 K).[2] Several experimental studies on bulk samples including measurements of resistivity, Hall effect, and magnetic properties arrived at the conclusion that the ground state of NiMnSb is half-metallic.[2,3] This was supported by the positron-annihilation measurements of bulk spin-polarization by Hanssen *et al.*[4]

In contrast, surface sensitive techniques, such as superconducting point contact measurements (Andreev reflection[5])[6,7] and spin-resolved photoemission spectroscopy[8,9] have failed to reproduce spin-polarization beyond the extent of a normal ferromagnet, even at low temperature. Calculations indicate NiMnSb surfaces and interfaces not to be half-metallic in general but using a suitably chosen interface—such as (111) oriented CdS or InP—half-metallicity can be restored.[10–12] Intersite disorder and point defects have also been suggested as a possible source for depolarization in, e.g., thin films.[13] *Ab initio* calculations by Alling *et al.*[14] have shown that interstitial defects, such as Mn or Ni occupying interstitial positions, are low in formation energy and that the former could explain the excess Mn consumption observed in certain preparation techniques[2] as well as the higher than expected magnetic moments.[15,16] However, such defects do not affect half-metallicity in the dilute regime. In fact, defects destroying half-metallicity have been found to be high in formation energy, making them unlikely to be present in NiMnSb at significant concentrations.[14,17] Energetically inexpensive defects induce states on the edges of the band gap but do not destroy the half-metallic character at low concentrations.

Bulk transport and magnetic properties of NiMnSb are reported to show an anomaly at 70–100 K, which has been interpreted as a transition from the half-metallic state to a metallic ferromagnetic state,[18] although its exact nature is far from clear. Several explanations have been suggested in the literature. Chioncel *et al.*[19,20] discussed the depolarization at finite temperature in terms of strong correlation effects out of reach of standard electronic structure methods. Recently such calculations were suggested to show that strong electron correlation effects suppress half-metallicity also at 0 K.[21] However, those calculations failed to reproduce experimental magnetic moments close to 4.0 μ_B, making their quantitative predictions questionable. Another line of explanation is thermal disordering of magnetic moments,[22] such as magnons. In a mathematical sense, any magnetic noncollinearity will destroy half-metallicity at any nonzero temperature.[23] It is debated whether the temperature 70–100 K really corresponds to a loss of half-metallicity or if the anomaly is of different origin. State of the art *ab initio* studies have shown the magnetization dynamics to be dominated by the Mn moment, with Ni only aligning itself to the fields of Mn atoms.[24] If Ni atoms could be replaced by other atoms with more robust magnetic moments and stronger magnetic interactions, the thermal dependence of magnetic properties of the material is likely to be altered.

NiMnSb is an ordered compound crystallizing in the so-called half-Heusler structure ($C1_b$), which is quite similar to the common semiconductor zinc-blende structure. Recently, we have shown that out of all choices of low concentration magnetic 3*d*-metal dopants in NiMnSb, Mn doping on the Ni site is one of the most promising candidates to improve finite temperature properties of NiMnSb.[25] This defect is favorable from a formation energy point-of-view under Mn-rich/Ni-

[a]Electronic mail: marekh@ifm.liu.se.

poor conditions, it preserves the half-metallic character of the band structure, and also induces strong magnetic interactions between Mn atoms sitting on the original Ni sites and their surroundings.[25] If the origin of the anomaly is related to thermal magnetic disorder, Mn alloying could raise the temperature where it occurs. Doping is also likely to have an impact on strong electron correlation effects.[19,20] However, if a high concentration of Mn replacing Ni is desired in the material, careful considerations must be made as regards the structural stability of the half-Heusler phase. The end compound Mn_2Sb, corresponding to all Ni atoms being replaced by Mn, crystallizes in the tetragonal C38 structure (Cu_2Sb-type) and is a normal metal.[26,27] If this crystal phase is obtained, the alloy cannot be expected to remain half-metallic.

In the present work we have performed *ab initio* calculations of ground state half-metallicity and magnetic properties for half-Heusler structured $Ni_{1-x}Mn_{1+x}Sb$ over the entire composition range, $0 \leq x \leq 1$. Its favorable properties motivates a study of the possibility for the alloy to be synthesized. Therefore, we have also performed a combined theoretical and experimental study of its structural stability with respect to the C38 crystal structure at finite temperature.

II. COMPUTATIONAL METHODOLOGY

The half-Heusler ($C1_b$) crystal structure of NiMnSb can be regarded as four interpenetrating fcc sublattices with the offsets $A=(0,0,0)$, $B=((1/4),(1/4),(1/4))$, $C=((1/2),(1/2),(1/2))$, and $D=((3/4),(3/4),(3/4))$ in terms of the lattice parameter. Sublattice A is occupied by Ni, B by Mn and D by Sb. Sublattice C is empty, in contrast to the *full* Heusler ($L2_1$) compounds, where it is occupied by an A-atom. In the literature we find the values 5.927 (Ref. 2) and 5.903 Å (Ref. 28) reported for the lattice constant. We consider doping sublattice A with Mn by removing Ni from the system and adding Mn. This defect will be denoted as "Mn_{Ni}."

In order to perform theoretical calculations for this system, we have employed a variety of *ab initio* methods. Density of states (DOS) and magnetic properties were calculated using a scalar-relativistic implementation of the exact muffin-tin orbitals (EMTOs) full charge density method. In combination with the coherent potential approximation (CPA),[29–32] this method allows for accurate and efficient modeling of chemically disordered systems. We used a basis set of s, p, and d muffin-tin orbitals and converged the total energy with respect to the number of **k**-points to within 0.1 meV per atom. Sublattice C was modeled as an empty atomic sphere at the ((1/2), (1/2), (1/2)) position of the unit cell.

We have calculated the pair exchange parameters, J_{ij}, of the Heisenberg Hamiltonian:

$$H_{\mathrm{ex}} = -\sum_{i \neq j} J_{ij} \hat{\mathbf{e}}_i \hat{\mathbf{e}}_j, \tag{1}$$

where $\hat{\mathbf{e}}_i$ is a unit vector pointing in the direction of the magnetic moment at site i. The physical meaning of J_{ij} is the cost in energy of rotating two spins at sites i and j by the angles $-\theta/2$ and $\theta/2$, keeping all other moments fixed. Positive sign indicates ferromagnetic spin alignment while negative sign indicates antiferromagnetic alignment. We have also determined the *effective* exchange parameter J_0, which measures the exchange energy cost of rotating one spin at site $i=0$ by the angle θ from its original orientation in a system with fixed moments. It can be written as:

$$J_0 = \sum_{j \neq 0} J_{0j}. \tag{2}$$

These quantities were calculated using the Liechtenstein–Katsnelson–Gubanov formula[33,34] within the EMTO framework from an ordered magnetic reference state. The use of a ferromagnetic (FM) state is justified since we are interested in *low* temperature behavior of the magnetic moments. In contrast, for calculations of the Curie temperature, the disordered local moment (DLM) state should be used instead.[35]

For thermodynamic considerations, we have modeled the $C1_b$–$Ni_{1-x}Mn_{1+x}Sb$ alloy as a mixture of the compounds $C1_b$–NiMnSb and $C1_b$–Mn_2Sb, where x is the fraction of $C1_b$–Mn_2Sb and consequently the concentration of substitutional Mn atoms on the Ni sublattice A. The isostructural mixing enthalpy in $C1_b$ crystal structure can then be defined as:

$$\Delta H(x) = H(x) - xH(\mathrm{Mn_2Sb}) - (1-x)H(\mathrm{NiMnSb}). \tag{3}$$

Including finite temperature, we have approximated the Gibbs free energy as:

$$\Delta G(x,T) = \Delta H(x) - TS(x), \tag{4}$$

where the entropy term, S, is approximated as:

$$S(x) = -k_{\mathrm{B}}[x \ln(x) + (1-x)\ln(1-x)]. \tag{5}$$

This is the mean-field approximation to the configurational entropy, and we neglect vibrational and magnetic entropy differences between the phases.

ΔH was calculated using the projector augmented waves (PAWs) (Ref. 36) method, as implemented in the VIENNA *AB INITIO SIMULATION PACKAGE*.[37,38] The disordered $C1_b$–$Ni_{1-x}Mn_{1+x}Sb$ alloys were modeled using supercells containing 48 and 72 atoms distributed according to the special quasirandom structure (SQS) technique.[39] We used a $5 \times 5 \times 5$ **k**-point mesh from which special points were chosen according to the Monkhorst–Pack scheme,[40] and the plane wave basis set cut-off energy 270 eV for $C1_b$ isostructural mixing enthalpy.

In order to investigate the thermodynamic stability of the $Ni_{1-x}Mn_{1+x}Sb$ alloy with respect to the $C1_b$ and C38 structures, we have calculated the energy differences:

$$\Delta E(\mathrm{NiMnSb}) = E^{\mathrm{C1_b}}(\mathrm{NiMnSb}) - E^{\mathrm{C38}}(\mathrm{NiMnSb}), \tag{6}$$

and

$$\Delta E(\mathrm{Mn_2Sb}) = E^{\mathrm{C1_b}}(\mathrm{Mn_2Sb}) - E^{\mathrm{C38}}(\mathrm{Mn_2Sb}). \tag{7}$$

The isostructural mixing enthalpies in the $C1_b$ and C38 structures can then be related to each other using the above energy differences.

The tetragonal C38 unit cell consists of six atoms at sites Ia: (0,0,0), Ib: (0.5, 0.5, 0), IIa: $(0,0.5,z)$, IIb: $(0.5,0,-z)$,

TABLE I. Lattice parameters obtained for the fully optimized C38–Mn_2Sb unit cell.

	a (Å)	c (Å)	z	z'
Theory (this work)	3.93	6.46	0.28	0.29
Experiment (Ref. 26)	4.078	6.557	0.295	0.280

IIIa: $(0,0.5,-z')$, and IIIb: $(0.5,0,z')$. We optimized the C38 structure by minimizing total energy with respect to the unit cell volume, while simultaneously relaxing a,c,z, and z' starting from the experimental values of Ref. 26. To this end we used a $25\times25\times25$ **k**-point mesh and the plane wave basis set cut-off energy 360 eV. Our obtained values of the lattice constants are given in Table I along with experimental values. When modeling NiMnSb in this structure we found the total energy to be minimized with Ni occupying sublattice I, Mn sublattice II and Sb occupying sublattice III, with the unit cell volume 17.5 $Å^3$/atom. C38–$Ni_{0.5}Mn_{1.5}Sb$ was modeled as an ordered compound with a Ni atom on sublattice I, providing us with an estimation of the mixing enthalpy for the disordered alloy. As will be evident in Sec. IV E of this study, the quantitative accuracy of the C38 phase mixing enthalpy is not as critical as for the $C1_b$ phase.

In our calculations we have employed the Perdew–Burke–Enzerhof (PBE) generalized gradient approximation (GGA) (Ref. 41) to the exchange-correlation functional. For the pure NiMnSb compound, we also performed EMTO calculations using the local density approximation while keeping the lattice constant fixed to the experimental value, which yielded results in good agreement with PBE-GGA at the calculated lattice constant.

We have also calculated formation energy of interstitial Mn defects in NiMnSb and $Ni_{0.5}Mn_{1.5}Sb$ by putting Mn on the empty sublattice C and then using the formula:

$$\Delta E = E^{\mathrm{def}} - E^{\mathrm{id}} + n\mu_0, \tag{8}$$

where E^{def} and E^{id} are the total energies of the unit cell with and without the defect, respectively. The third term on the right hand side takes into account that when forming the defects, n atoms are taken from a reservoir of chemical potential μ_0. In this work we have used the simple antiferromagnetic fcc-Mn as a reservoir. We neglect formation of different crystal phases when considering this defect, since our primary interest is if the tendency of Mn interstitial formation will be increased or decreased in $C1_b$–$Ni_{0.5}Mn_{1.5}Sb$ compared to $C1_b$–NiMnSb, making the particular choice of μ_0 less critical. The Mn defects were distributed quasirandomly on sublattice C, and ΔE was then calculated using the locally self-consistent Green's function (LSGF) method[42] for a supercell consisting of $5\times5\times5$ unit cells.

III. EXPERIMENTAL METHODOLOGY

We have performed simultaneous direct current (dc) magnetron sputtering of NiSb, MnSb, and Mn targets using three 2 in. magnetrons in a confocal sputter-down arrangement with 11 cm target to substrate distance. Target purity was 99.9 wt. % for the alloys and 99.95 wt % for Mn. During the deposition process the dc cathode currents were kept at constant values adjusted to give a stoichiometric NiMnSb film at the center of the substrate table. This was achieved using the values I_{NiSb}=49 mA, I_{MnSb}=41 mA, and I_{Mn}=30 mA. By choosing off-center positions, the film composition could be controlled and films with different compositions could be grown under the same external conditions. The films were deposited on 5×5 mm^2 MgO(100) substrates, which were cleaned in an ultrasonic bath of acetone, followed by isopropanol. A final cleaning step consisted of heating to 400 °C during one hour prior to deposition. During deposition, the substrate was heated to 315 °C and was kept at floating potential. The chamber background pressure was $3-8\times10^{-7}$ Torr and we performed the deposition in an Ar-atmosphere at 5.0 mTorr pressure.

We estimated the deposition rate by studying fractures of films grown on larger Si(111) substrates using scanning electron microscopy. In order to determine the film compositions we have used energy-dispersive x-ray spectroscopy (EDX), which has an accuracy of the order of 1 at. %. The crystal structure was investigated using x-ray diffraction in grazing incidence configuration (GIXRD) with a Philips X'pert MRD diffractometer using Cu K_α radiation. The peaks were fitted to a Gaussian and lattice constants were obtained as a weighted average over the three most intense peaks of the GIXRD diffractograms. We estimated the error in the lattice constant by considering the obtained value for the lattice constant and a value adjusted for the zero-point offset in the measurement. The errors were then estimated by taking the weighted average between this deviation for each peak.

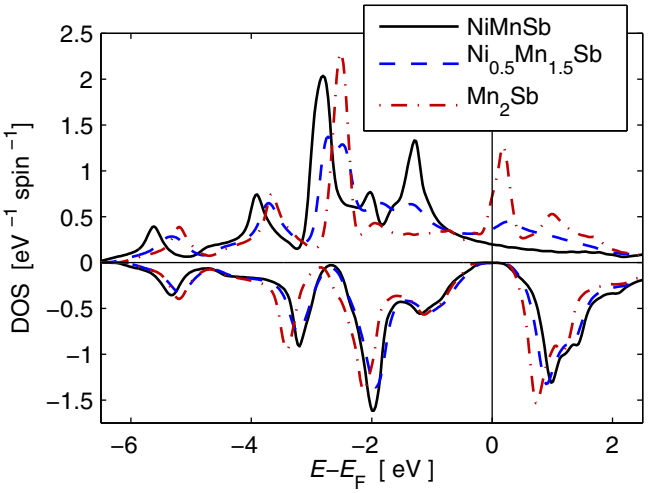

FIG. 1. (Color online) Spin-resolved DOS for NiMnSb, $Ni_{0.50}Mn_{1.50}Sb$ and Mn_2Sb in the $C1_b$ half-Heusler structure, calculated with the EMTO-CPA method. The Fermi level, indicated by the vertical black line, is centered in the spin down band gap which is insensitive to Mn_{Ni} concentration.

IV. RESULTS AND DISCUSSION

A. DOS

Figure 1 shows calculated spin-resolved DOS for $C1_b$–NiMnSb, $Ni_{0.50}Mn_{1.50}Sb$, and Mn_2Sb. The spin down band gap centered on the Fermi level is clearly visible for NiMnSb, in agreement with previous work.[1,14] As Ni is re-

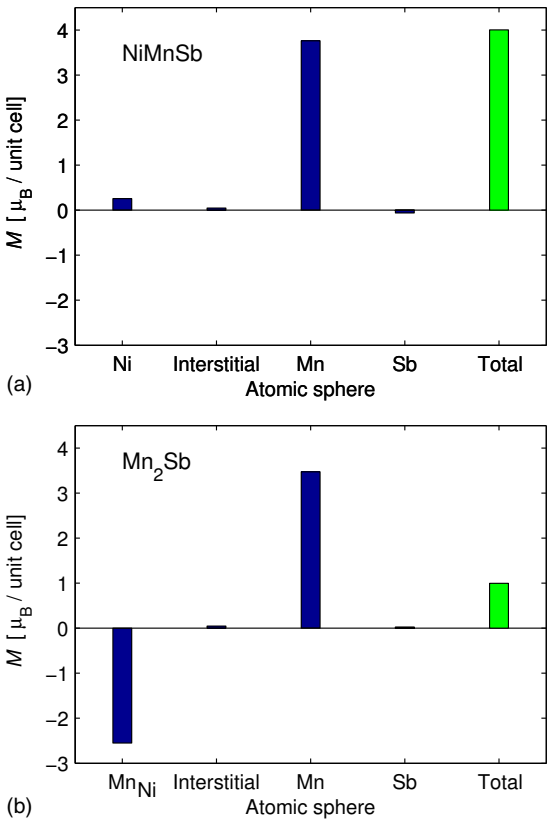

FIG. 2. (Color online) Total magnetic moments per crystallographic unit cell for (a) $C1_b$–NiMnSb and (b) $C1_b$–Mn_2Sb, along with site-resolved moments. The integer total moment is a necessary condition for half-metallic compounds.

placed by Mn, the most significant feature is that the band gap remains intact, even for Mn_2Sb. The spin down bonding and antibonding states are of Ni *d* and Mn *d* character, respectively. For the artificial compound $C1_b$–Mn_2Sb, we obtain a large peak just above the Fermi level in the spin up band. The insensitivity of the band gap to Mn surplus makes intentional doping in this way particularly attractive.

B. Magnetic moments

We have calculated magnetic moments for the NiMnSb and Mn_2Sb compounds in the $C1_b$ structure. The results are shown in Fig. 2, which also displays the moments resolved for each atomic sphere. The total magnetic moment of NiMnSb is the integer 4.0 μ_B per unit cell, in agreement with previous calculations.[1] In terms of Bohr magnetons, this is equal to the number of unpaired spins and reflects its full spin-polarization at the Fermi level, as all spin down bonding states are filled. Integer total spin magnetic moment per unit cell is in fact a necessary condition for half-metallic compounds.[43] The magnetic moment is almost entirely localized to the Mn atomic sphere while Ni carries only a small moment. When replacing Ni with Mn, three electrons are removed from the unit cell. These are taken exclusively from the spin up band, reducing the total moment to 1 μ_B for $C1_b$–Mn_2Sb, as seen in Fig. 2(b). Consequently, $C1_b$–Mn_2Sb is also half-metallic, in line with the discussion in Ref. 43, and evidenced by the direct DOS calculations of Fig. 1. The local magnetic moment of Mn is virtually unaffected by this substitution and the Mn atoms sitting on sublattice *A*, denoted as Mn_{Ni}, obtain a large negative moment. However, as indicated in Fig. 1, this negative moment does not involve spin down states at the Fermi level.

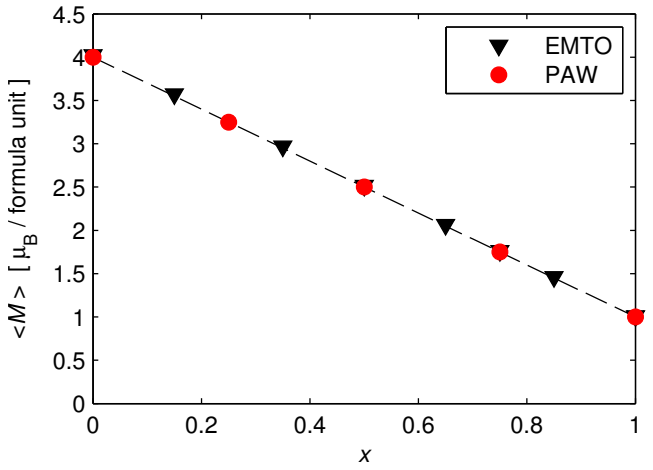

FIG. 3. (Color online) Average magnetic moment per cell for $C1_b$–$Ni_{1-x}Mn_{1+x}Sb$ as a function of Mn surplus, *x*, calculated with the EMTO-CPA and PAW methods, the latter including local lattice relaxations. The strictly linear relation indicates half-metallicity at all compositions.

We now extend the discussion of total magnetic moments to $C1_b$–$Ni_{1-x}Mn_{1+x}Sb$ alloys by showing in Fig. 3 the total magnetic moment, calculated with the EMTO-CPA and PAW supercell methods, averaged over all crystallographic unit cells as a function of composition, *x*. This average total moment, $\langle M \rangle$, shows a linear dependence on composition, summarized by the formula:

$$\langle M \rangle = M^{\mathrm{NiMnSb}} - 3x = 4 - 3x. \tag{9}$$

The linearity is a reflection of half-metallicity for the alloy systems, as the electrons are progressively removed only from the spin up band. It should be pointed out that although the average moment is noninteger the total supercell moment is still an integer and as shown by the DOS calculations in Fig. 1, the alloys retain half-metallicity, like the parent compounds $C1_b$–NiMnSb and $C1_b$–Mn_2Sb.

C. Exchange interactions

In order to investigate the stability of the magnetic ground state with respect to thermal excitations we have calculated the effective exchange parameter J_0, defined in Eq. (2), which describes the cost in energy of deviating a single moment in the ground state environment. The results are shown in Fig. 4 for Ni, Mn, and Mn_{Ni}. The Ni J_0 is the smallest, reflecting the weak coupling of the Ni moment to its environment. Mn_{Ni} shows almost an order of magnitude stronger coupling. In our sign convention the positive sign of J_0 for Mn_{Ni} indicates a stable magnetic moment, although antiparallel to the total magnetic moment. The Mn J_0 is also large and increases with Mn_{Ni} concentration.

In Fig. 5 we show pair exchange parameters, J_{ij}, in $C1_b$–NiMnSb. This quantity can be considered as a measure of the coupling strength between local moments, and is defined in Eq. (1). The strongest interaction is between Mn moments on sublattice *B*. Ni–Mn coupling is half as strong

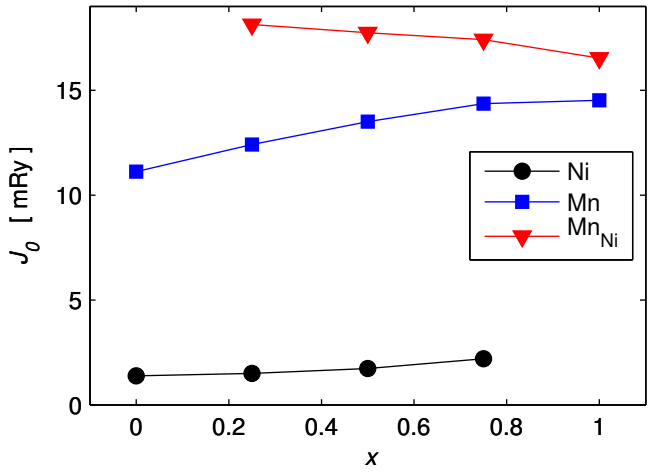

FIG. 4. (Color online) Effective magnetic exchange parameter, J_0, for Ni, Mn, and Mn_{Ni} in $C1_b-Ni_{1-x}Mn_{1+x}Sb$.

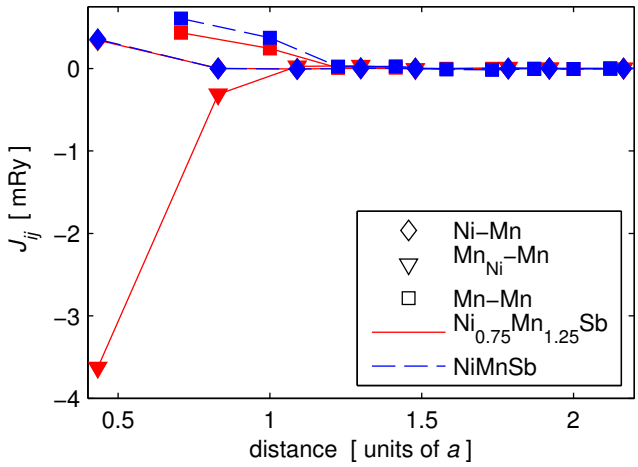

FIG. 6. (Color online) Pair exchange parameters in $C1_b-Ni_{0.75}Mn_{1.25}Sb$ and NiMnSb. Mn atoms on the Ni sublattice (Mn_{Ni}) couple very strongly to host Mn atoms.

and between Ni moments there is only negligible coupling. It should be noted that there are only four Ni–Mn nearest-neighbors, as opposed to 12 Mn–Mn nearest-neighbors. Our results are qualitatively in agreement with the results in Refs. 25 and 44.

When Ni atoms are replaced by Mn we observe an extremely strong intersublattice exchange coupling between Mn_{Ni} and Mn atoms, as shown in Fig. 6 for 25% Mn surplus. This is almost one order of magnitude stronger than the coupling between Ni and the Mn sublattice (B), which is roughly constant. We note that the $Mn-Mn_{Ni}$ coupling is antiferromagnetic, as reflected in Fig. 2(b). Figure 7 shows the concentration dependence of selected J_{ij}'s. With increasing Mn_{Ni} concentration, the $Mn_{Ni}-Mn$ coupling decreases as does the Mn–Mn coupling. The intrasublattice coupling between Mn_{Ni} moments is rather weak—although stronger than the Ni–Ni coupling, as shown in Fig. 5 and shows a slight increase with Mn_{Ni}-concentration.

In summary, our study of magnetic properties of $C1_b-Ni_{1-x}Mn_{1+x}Sb$ solid solutions indicates that Mn surplus on Ni sublattice strengthens magnetic interactions in the system while preserving half-metallic properties. It is therefore a highly interesting question if such a system can be synthesized. In the remaining parts of this paper, we will therefore address this question theoretically as well as experimentally.

D. Isostructural mixing enthalpy

The $C1_b-Ni_{1-x}Mn_{1+x}Sb$ alloy can be regarded as a mixture of $C1_b-NiMnSb$ and $C1_b-Mn_2Sb$. In order to investigate its stability with respect to decomposition into these constituents, we have calculated the isostructural mixing enthalpy, as defined in Eq. (3), for $C1_b-Ni_{1-x}Mn_{1+x}Sb$ using the PAW method. The results are shown in Fig. 8. Keeping the lattice static yields a small mixing enthalpy that is negative and decreases to −4.8 meV/f.u. as x approaches 0.75. The negative sign indicates the tendency toward spontaneous mixing, while the small absolute value indicates this tendency to be relatively weak. Including local lattice relaxations lowers the mixing enthalpy of $C1_b-Ni_{0.25}Mn_{1.75}Sb$ by a further 5.4 meV/f.u., which is substantial on this small scale. The mixing enthalpy assumes its minimum of almost −12 meV/f.u. between $x=0.5$ and $x=0.75$. Thus, the $C1_b$ $Ni_{1-x}Mn_{1+x}Sb$ alloy can be considered stable with respect to isostructural decomposition into $C1_b-NiMnSb$ and $C1_b-Mn_2Sb$ phases, which strongly advocates the possibility

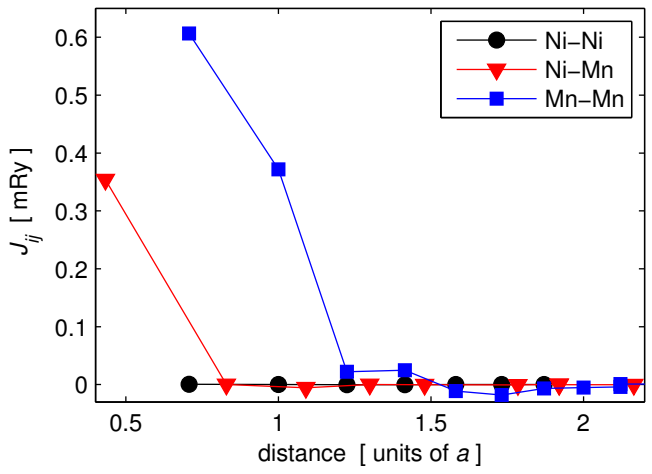

FIG. 5. (Color online) Magnetic pair exchange parameters in $C1_b-NiMnSb$.

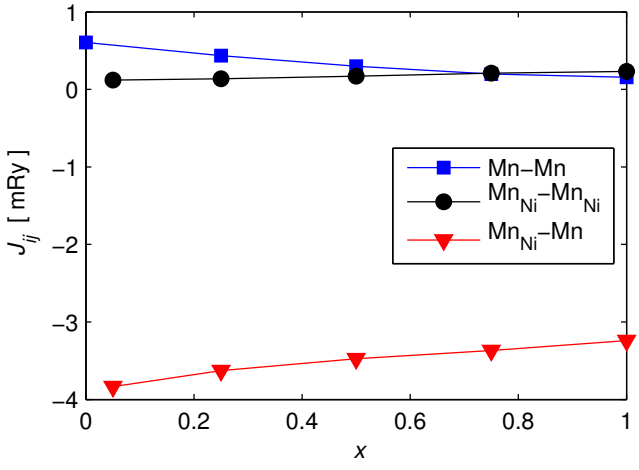

FIG. 7. (Color online) Concentration dependence of nearest-neighbor pair exchange parameters in $C1_b-Ni_{1-x}Mn_{1+x}Sb$.

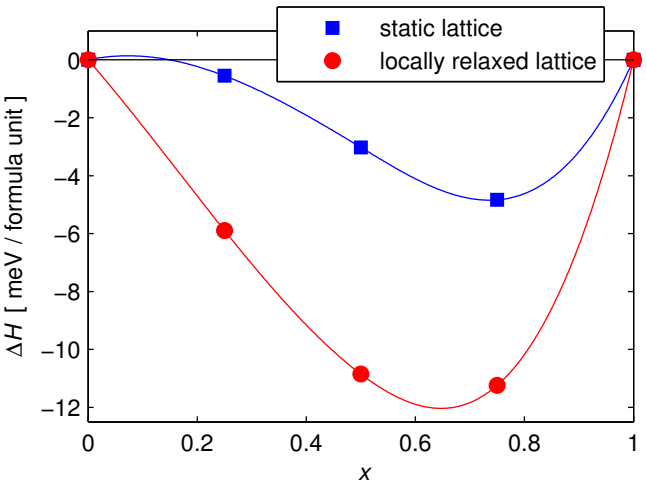

FIG. 8. (Color online) Mixing enthalpy for $C1_b$–$Ni_{1-x}Mn_{1+x}Sb$ with respect to $C1_b$–NiMnSb and $C1_b$–Mn_2Sb, calculated within two approximations: keeping the lattice static and including local lattice relaxations. The negative sign indicates the tendency of spontaneous mixing.

of synthesizing this material. Indeed, thin film synthesis has proved successful for solid solutions using even materials with strong tendency toward isostructural decomposition.[45,46] We will now investigate the stability of the alloy with respect to the competing C38 phase at finite temperature.

E. Structural stability at finite temperature

Adding configurational entropy evaluated within the mean-field approximation of Eq. (5) to the mixing enthalpy, and calculating the relative energy differences between the end compounds NiMnSb and Mn_2Sb in the $C1_b$ and C38 structures, we obtain the Gibbs free energy of mixing, $\Delta G(T)$, for $Ni_{1-x}Mn_{1+x}Sb$ at finite temperature in the two crystal structures. The results are shown in Fig. 9 for $T_1=0$ K, $T_2=600$ K, and $T_3=1500$ K, which is 100 K above the melting point of 1400 K for NiMnSb.[2,3] In order to estimate the amount of Mn that can be incorporated in the $C1_b$ crystal structure by replacing Ni, we have drawn the Gibbs common tangent line to the curves corresponding to $T=600$ K—which is a common sputter deposition temperature for NiMnSb. We find the left tangent point to be located at $x=0.32$, which implies that up to 32% extra Mn can be incorporated in the $C1_b$ structure without resulting in any secondary C38 crystal phase formation. At slightly higher concentration, the driving force—i.e., the difference in energy between the tangent line and the $C1_b$ structure ΔG-curve—is still small, and it should be possible to overcome this energy barrier via nonequilibrium growth techniques.

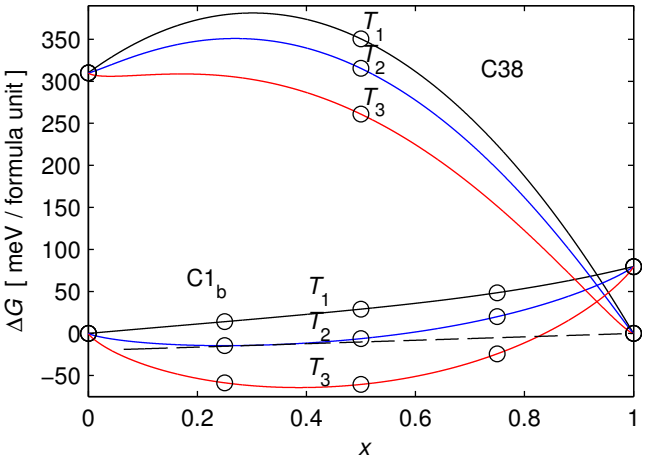

FIG. 9. (Color online) Gibbs free energy of $Ni_{1-x}Mn_{1+x}Sb$ calculated in the $C1_b$ and C38 crystal structures at the temperatures $T_1=0$ K, $T_2=600$ K, and $T_3=1500$ K. The dashed line is the Gibbs common tangent construction for $T=T_2$. Circles indicate points obtained from direct calculation.

Although the main focus of the present paper does not lie in the very high temperature regime, we have included the Gibbs free energy corresponding to 1500 K (T_3) in Fig. 9, as this may be of relevance for preparation of the $C1_b$–$Ni_{1-x}Mn_{1+x}Sb$ alloy by melting. By the common tangent construction we find that over 60% Mn can be incorporated in the $C1_b$ crystal structure at this temperature. However, since this temperature is far above the Curie point for NiMnSb of 728 K, one may expect the magnitude of the isostructural mixing enthalpy, ΔH, to be affected by strong thermal disordering of local magnetic moments, a phenomenon observed in Ref. 47. Our results concerning synthesis by melting may yet serve as a first approximation, opening the door to future study. Furthermore, it should be pointed out in reference to both T_2 and T_3 that use of the mean-field approximation will underestimate the stability of solid solutions, and will consequently underestimate the solubility limits.

Based on the above results, we predict that $Ni_{1-x}Mn_{1+x}Sb$ indeed can be synthesized in the $C1_b$ structure with substantial concentrations of Mn_{Ni} defects.

F. Sputter deposition

In order to test our predictions concerning the crystal phase stability presented in Sec. IV E, we have performed dc magnetron sputtering of NiSb, MnSb, and Mn targets simultaneously using MgO(100) substrates. The deposition was carried out during 60 min with an average deposition rate of 2.3 Å/s. We have determined the resulting film compositions using EDX, which are presented in Table II. It should again be pointed out that the accuracy of EDX is in the order of ~1 at. %. For sample 1 we managed to obtain near-stoichiometric composition and in sample 2, the composition corresponds to $x\approx0.19$, i.e., about 19% Mn surplus.

In order to investigate the structural phases residing in the samples we have performed GIXRD measurements. The results for samples 1 and 2 are shown in Fig. 10. For sample 1, with near-stoichiometric composition, we find the peak positions to coincide to large extent with tabulated values for $C1_b$–NiMnSb.[48,49] The diffraction peak positions corresponding to the C38–Mn_2Sb structure[50] are also indicated in Fig. 10. However, they do not coincide with our observed diffraction pattern. The diffractogram of sample 2, containing approximately 19% Mn surplus, does coincide with the pattern of the $C1_b$ crystal structure. Some peaks are suppressed and some are enhanced compared to sample 1, implying a change in texture or chemical disorder with composition.

TABLE II. Compositions and lattice constants of $Ni_{1-x}Mn_{1+x}Sb/MgO(100)$ films grown by magnetron sputtering.

Sample No.	Deposition time (min)	Composition (%)				a (Å)
		Ni	Mn	Sb	x	
1	60	31.5	34.5	34.0	0.046	5.918
2	60	27.6	40.6	31.8	0.19	5.954
3	30	⋯	⋯	⋯	⋯	5.927
4	30	⋯	⋯	⋯	⋯	5.950

The lattice constants of samples 1 and 2 are given in Table II and are also plotted in Fig. 11 together with literature values and our theoretical results obtained using the PAW, EMTO, and LSGF methods. Our obtained values for the near-stoichiometric sample are in good agreement with both theory and experimental references for NiMnSb. Calculations indicate an approximately linear increase in lattice constant as a function of substitutional Mn composition. Our experimental results also reveal an increase with composition, which is steeper than predicted by theory. It should be noted that the calculations assume disorder only on sublattice A, while in our samples we must expect to have some chemical disorder also on the other sublattices.

We have also grown two films under the same conditions as samples 1 and 2 but with only 30 min deposition time. We therefore expect the compositions of these samples (3 and 4) to be approximately the same as of samples 1 and 2, respectively. Figure 12 shows the GIXRD diffraction patterns of samples 3 and 4. For the near-stoichiometric film (sample 3), the pattern is qualitatively very similar to that of sample 1. With respect to peak positions, this is also the case for sample 4, that is similar to sample 2. The lattice constants, presented in Table II, were deduced from the diffraction patterns and are very similar to samples 1 and 2. Increasing Mn composition (sample 4), the change in pattern is much smaller than for the thicker films, and is mostly concerned with small shifts in relative peak heights. The absence of any peaks that cannot be explained by the $C1_b$ structure in any of our four samples leads us to the conclusion that substantial amounts of Mn indeed can be included in the alloy without obtaining the C38 structure, in agreement with the predictions in Sec. IV E.

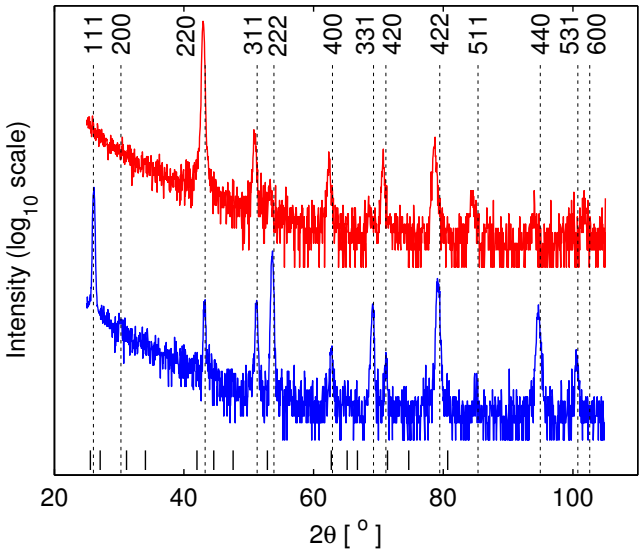

FIG. 10. (Color online) GIXRD pattern for $Ni_{1-x}Mn_{1+x}Sb/MgO(100)$ sample 1 with near-stoichiometric composition (bottom), and sample 2 with Mn surplus corresponding to $x \approx 0.19$ (top). The marks above the x-axis correspond to the tabulated diffraction peaks of C38–Mn_2Sb (Ref. 50). Dashed lines indicate powder diffraction peaks of $C1_b$–NiMnSb with lattice constant 5.903 Å (Ref. 48) along with the corresponding Miller indices.

G. Interstitial Mn defects

We interpret the increased composition dependence of the lattice constant for the Mn enriched sample, shown in Fig. 11, as an indication of chemical disorder in the samples. Previous experimental and theoretical[14] studies have shown Mn interstitial defects likely to occur. A full investigation of the mutual interplay of all possible defects is beyond the scope of the present paper. However, we have investigated the influence of Mn_{Ni} doping on the formation energy of interstitial Mn defects from *ab initio* calculations. To this end we put Mn atoms on 5% of the empty sites of sublattice C and calculated the average formation energy per Mn atom in the $C1_b$-structured systems NiMnSb and $Ni_{0.50}Mn_{1.50}Sb$. The formation energy of such defects in NiMnSb is 1.3 eV, as presented in Table III. It should be added that this value is higher than reported in Ref. 14, which is due to the use of a

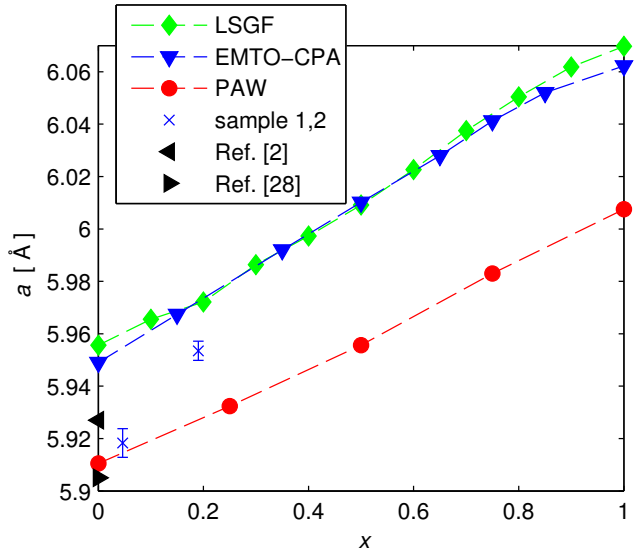

FIG. 11. (Color online) Lattice parameters of samples 1 and 2 together with theoretical results and literature values for $C1_b$–$Ni_{1-x}Mn_{1+x}Sb$.

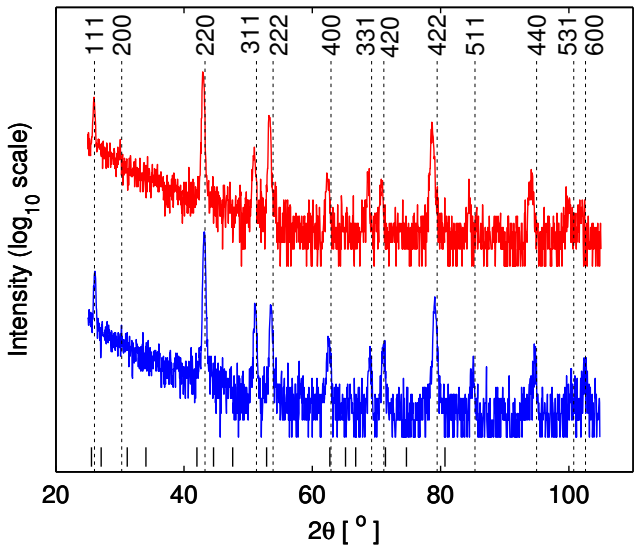

FIG. 12. (Color online) GIXRD pattern for $Ni_{1-x}Mn_{1+x}Sb/MgO(100)$ sample 3 with near-stoichiometric composition (bottom), and sample 4 with Mn surplus (top). The vertical marks and lines have the same meaning as in Fig. 10.

different exchange-correlation functional. The value presented in Ref. 25 is also lower but was obtained with the PAW method and included local lattice relaxations. In any case, the formation energy of Mn interstitial defects in $Ni_{0.50}Mn_{1.50}Sb$ is found to be 0.1 eV lower than in NiMnSb. This difference is very small compared to the absolute value as well as to the formation energies of other defects in NiMnSb.[14,25] Based on these facts, we do not anticipate significantly higher concentration of interstitial Mn defects in the $Ni_{1-x}Mn_{1+x}Sb$ alloy for $x \leq 0.5$ than in the NiMnSb compound.

V. SUMMARY AND CONCLUSIONS

We have investigated the possibility of synthesizing $Ni_{1-x}Mn_{1+x}Sb$ alloy in the $C1_b$ half-Heusler crystal structure by means of *ab initio* calculations and magnetron sputter deposition. Calculations indicate that the half-metallic band gap of the spin down channel is unaffected by the substitution of Mn for Ni, and that the Mn magnetic moments of the atoms replacing Ni couple very strongly to the original Mn sublattice. We have grown films with ~19% Mn surplus/Ni deficit, and we obtain the x-ray diffraction pattern expected for the $C1_b$ crystal structure with a slight increase in lattice spacing which is in line with calculations for the solid solution. We see no diffraction peaks corresponding to the competing tetragonal C38 phase—which is the ground-state structure of Mn_2Sb—that cannot be conferred to the $C1_b$ crystal structure. From these results we conclude that the Mn-rich alloy indeed can be synthesized in the desired crystal structure, which opens the door to engineering magnetic and electrical properties of Mn-rich half-Heusler compounds by alloying.

ACKNOWLEDGMENTS

We gratefully acknowledge Dr. Sergei I. Simak for help with SQS supercell construction as well as Ulrika Isaksson and Mattias Samuelsson for help with x-ray diffraction measurements. Financial support from the Swedish Research Council (VR) and the Göran Gustafsson Foundation for Research in Natural Sciences and Medicine is gratefully acknowledged. Calculations have been carried out at the facilities of the National Supercomputer Centre in Linköping, Sweden.

TABLE III. Average formation energy per Mn-atom calculated for 5% interstitial Mn defects in the $C1_b$–NiMnSb and $C1_b$–$Ni_{0.5}Mn_{1.5}Sb$ alloys.

Host	ΔE (eV)
NiMnSb	1.3
$Ni_{0.5}Mn_{1.5}Sb$	1.2

[1] R. A. de Groot, F. M. Mueller, P. G. van Engen, and K. H. J. Buschow, Phys. Rev. Lett. **50**, 2024 (1983).
[2] M. J. Otto, R. A. M. van Woerden, P. J. van der Valk, J. Wijngaard, C. F. van Bruggen, C. Haas, and K. H. J. Buschow, J. Phys.: Condens. Matter **1**, 2341 (1989).
[3] M. J. Otto, R. A. M. van Woerden, P. J. van der Valk, J. Wijngaard, C. F. van Bruggen, and C. Haas, J. Phys.: Condens. Matter **1**, 2351 (1989).
[4] K. E. H. M. Hanssen, P. E. Mijnarends, L. P. L. M. Rabou, and K. H. J. Buschow, Phys. Rev. B **42**, 1533 (1990).
[5] R. J. Soulen, Jr., M. S. Osofsky, B. Nadgorny, T. Ambrose, P. Broussard, S. F. Cheng, J. Byers, C. T. Tanaka, J. Nowack, J. S. Moodera, G. Laprade, A. Barry, and M. D. Coey, J. Appl. Phys. **85**, 4589 (1999).
[6] R. J. Soulen, Jr., J. M. Byers, M. S. Osofsky, B. Nadgorny, T. Ambrose, S. F. Cheng, P. R. Broussard, C. T. Tanaka, J. Nowak, J. S. Moodera, A. Barry, and J. M. D. Coey, Science **282**, 85 (1998).
[7] S. K. Clowes, Y. Miyoshi, Y. Bugoslavsky, W. R. Branford, C. Grigorescu, S. A. Manea, O. Monnereau, and L. F. Cohen, Phys. Rev. B **69**, 214425 (2004).
[8] W. Zhu, B. Sinkovic, E. Vescovo, C. Tanaka, and J. S. Moodera, Phys. Rev. B **64**, 060403 (2001).
[9] M. Sicot, P. Turban, S. Andrieu, A. Tagliaferri, C. De Nadai, N. Brookes, F. Bertran, and F. Fortuna, J. Magn. Magn. Mater. **303**, 54 (2006).
[10] G. A. de Wijs and R. A. de Groot, Phys. Rev. B **64**, 020402 (2001).
[11] I. Galanakis, M. Ležaić, G. Bihlmayer, and S. Blügel, Phys. Rev. B **71**, 214431 (2005).
[12] J. J. Attema, G. A. de Wijs, and R. A. de Groot, J. Phys. D: Appl. Phys. **39**, 793 (2006).
[13] D. Orgassa, H. Fujiwara, T. C. Schultess, and W. H. Butler, J. Appl. Phys. **87**, 5870 (2000).
[14] B. Alling, S. Shallcross, and I. A. Abrikosov, Phys. Rev. B **73**, 064418 (2006).
[15] C. N. Borca, T. Komesu, H.-K. Jeong, P. A. Dowben, D. Ristoiu, C. Hordequin, J. P. Nozières, J. Pierre, S. Stadler, and Y. U. Idzerda, Phys. Rev. B **64**, 052409 (2001).
[16] L. Ritchie, G. Xiao, Y. Ji, T. Y. Chen, C. L. Chien, M. Zhang, J. Chen, Z. Liu, G. Wu, and X. X. Zhang, Phys. Rev. B **68**, 104430 (2003).
[17] J. J. Attema, C. M. Fang, L. Chioncel, G. A. de Wijs, A. I. Lichtenstein, and R. A. de Groot, J. Phys.: Condens. Matter **16**, S5517 (2004).
[18] C. Hordequin, D. Ristoiu, L. Ranno, and J. Pierre, Eur. Phys. J. B **16**, 287 (2000).
[19] L. Chioncel, M. I. Katsnelson, R. A. de Groot, and A. I. Lichtenstein, Phys. Rev. B **68**, 144425 (2003).
[20] L. Chioncel, E. Arrigoni, M. I. Katsnelson, and A. I. Lichtenstein, Phys. Rev. Lett. **96**, 137203 (2006).
[21] H. Allmaier, L. Chioncel, E. Arrigoni, M. I. Katsnelson, and A. I. Lichtenstein, Phys. Rev. B **81**, 054422 (2010).
[22] P. A. Dowben and R. Skomski, J. Appl. Phys. **93**, 7948 (2003).
[23] L. M. Sandratskii, Phys. Rev. B **78**, 094425 (2008).
[24] P. Buczek, A. Ernst, P. Bruno, and L. M. Sandratskii, Phys. Rev. Lett. **102**, 247206 (2009).
[25] B. Alling, M. Ekholm, and I. A. Abrikosov, Phys. Rev. B **77**, 144414 (2008).
[26] L. Heaton and N. S. Gingrich, Acta Crystallogr. **8**, 207 (1955).
[27] J. H. Wijngaard, C. Haas, and R. A. de Groot, Phys. Rev. B **45**, 5395

(1992).
[28]L. Castelliz, Monatsch. Chem. **82**, 1059 (1951).
[29]L. Vitos, I. A. Abrikosov, and B. Johansson, in *Complex Inorganic Solids*, edited by P. E. A. Turchi, A. Gonis, K. Rajan, and A. Meike (Springer, New York, 2005).
[30]L. Vitos, Phys. Rev. B **64**, 014107 (2001).
[31]L. Vitos, I. A. Abrikosov, and B. Johansson, Phys. Rev. Lett. **87**, 156401 (2001).
[32]L. Vitos, *Computational Quantum Mechanics for Materials Engineers: The EMTO Method and Applications* (Springer-Verlag, London, 2007).
[33]A. I. Liechtenstein, M. I. Katsnelson, V. P. Antropov, and V. A. Gubanov, J. Magn. Magn. Mater. **67**, 65 (1987).
[34]A. I. Liechtenstein, M. I. Katsnelson, and V. A. Gubanov, J. Phys. F: Met. Phys. **14**, L125 (1984).
[35]B. Alling, A. V. Ruban, and I. A. Abrikosov, Phys. Rev. B **79**, 134417 (2009).
[36]P. E. Blöchl, Phys. Rev. B **50**, 17953 (1994).
[37]G. Kresse and J. Furthmüller, Phys. Rev. B **54**, 11169 (1996); G. Kresse and J. Furthmüller, *ibid.* **49**, 14251 (1994).
[38]G. Kresse and J. Furthmüller, Comput. Mat. Sci. **6**, 15 (1996).
[39]A. Zunger, S. H. Wei, L. G. Ferreira, and J. E. Bernard, Phys. Rev. Lett. **65**, 353 (1990).
[40]H. J. Monkhorst and J. D. Pack, Phys. Rev. B **13**, 5188 (1976).
[41]J. P. Perdew, K. Burke, and M. Ernzerhof, Phys. Rev. Lett. **77**, 3865 (1996).
[42]I. A. Abrikosov, A. M. N. Niklasson, S. I. Simak, B. Johansson, A. V. Ruban, and H. L. Skriver, Phys. Rev. Lett. **76**, 4203 (1996).
[43]R. A. de Groot, Physica B **172**, 45 (1991).
[44]E. Şaşıoğlu, L. M. Sandratskii, P. Bruno, and I. Galanakis, Phys. Rev. B **72**, 184415 (2005).
[45]P. Eklund, M. Beckers, U. Jansson, H. Högberg, and L. Hultman, Thin Solid Films **518**, 1851 (2010).
[46]H. Holleck, Surf. Coat. Technol. **36**, 151 (1988).
[47]P. Olsson, I. A. Abrikosov, L. Vitos, and J. Wallenius, J. Nucl. Mater. **321**, 84 (2003).
[48]Powder Diffraction File Card No. 06-0677, Joint Committee on Powder Diffraction Standards (JCPDS)-International Centre for Diffraction Data (1998).
[49]The $2\theta=101°$ and 103° peaks were indexed by us as (531) and (600), respectively, based on calculations.
[50]Powder Diffraction File Card No. 04-0822, Joint Committee on Powder Diffraction Standards (JCPDS)-International Centre for Diffraction Data (1998).